Available online at www.sciencedirect.com
ScienceDirect
ELSEVIER
June 2010, 17(3): 38–44
www.sciencedirect.com/science/journal/10058885
The Journal of China Universities of Posts and Telecommunications
http://www.jcupt.com

Spatial characteristics and capacity investigation of indoor hotspot channel based on wideband MIMO measurement at 4.9 GHz

NIE Xin[1,2] (✉), ZHANG Jian-hua[1,2], HUANG Chen[2], LIU Ze-min[1], ZHANG Ping[1,2]

1. Key Laboratory of Universal Wireless Communications, Ministry of Education, Beijing University of Posts and Telecommunications, Beijing 100876, China
2. Wireless Technology Innovation Institute, Beijing University of Posts and Telecommunications, Beijing 100876, China

Abstract

In this article, results obtained from wideband multiple-input multiple-output channel measurements at 4.9 GHz are presented. Measurements were performed in an indoor hotspot scenario with both line-of-sight and non-line-of-sight propagation conditions. Vertical polarized uniform linear arrays (ULAs) with different antenna spacing and orientation were utilized for investigating the impact of antenna configurations on the system performance. Based on measured channel impulse responses, the spatial correlation of ULA is analyzed and compared with the theoretical values calculated from the power azimuth spectrum. Following that, the eigenvalue statistics and capacity with respect to antenna spacing and orientation are given and compared. The diversity-multiplexing tradeoff (DMT) of measured channels at operational signal-to-noise ratio (SNR) is also presented. The reason why the DMT of measured channels is much lower than that of i.i.d. Rayleigh channels is specified.

Keywords wideband multiple-input multiple-output (MIMO) measurement, indoor hotspot scenario, spatial characteristics, capacity

1 Introduction

MIMO, which has high spectral efficiency and reliability [1–2], is one of the most promising 4G candidate technologies. An important application of MIMO system occurs in indoor hotspot scenario with heavy traffic and high user density, such as conference halls, shopping malls and airports. Performance of MIMO system is essentially influenced by statistics of propagation channel between transmitter (Tx) array and receiver (Rx) array. Thus, extensive investigations based on measurement are vital for MIMO channel modeling and performance evaluation in real channel environment.

Several narrowband indoor MIMO channel measurements were reported by earlier works [3–4]. These measurements were conducted in different indoor scenarios at center frequencies of 2 GHz, 5.2 GHz, and 5.8 GHz, respectively. The correlation properties of large-scale fading of narrowband channel at 1.8 GHz and wideband channel at 5.2 GHz with 120 MHz bandwidth were presented in Ref. [5]. The effect of different antennas on the mutual information of narrow channel was analyzed in Ref. [6]. In Ref. [7], the results of spatial correlation and capacity in an office environment with fixed antenna configuration at 5 GHz were reported. Due to the differences in frequency band, antenna configurations, layout of buildings and building materials, the propagation channels exhibit different characteristics. Moreover, the analysis concerning the impact of antenna configurations on wideband MIMO channel is scarce. Thus, a more comprehensive experimental investigation is needed.

The authors conducted a measurement campaign to explore the statistics of indoor hotspot MIMO channel at 4.9 GHz in China. They focus on the spatial characteristics of wideband MIMO channel. The impact of antenna configuration on wideband channel is their main concern. The main contributions of this article consist in:

1) The analysis of the spatial correlation statistics of the wideband MIMO channel.

2) The investigation of eigenvalue dispersion and capacity results of wideband MIMO channel.

3) The impact of antenna spacing and array orientation on MIMO performance.

4) The DMT at the typical operational SNR in real propagation environment.

The remainder of this article is organized as follows. Sect. 2 describes the measurement equipments and environment. Sect. 3

Received date: 01-06-2009
Corresponding author: NIE Xin, E-mail: niexin1983@gmail.com
DOI: 10.1016/S1005-8885(09)60466-0

?1994-2014 China Academic Journal Electronic Publishing House. All rights reserved. http://www.cnki.net

shows the procedure of data post-processing. Sect. 4 presents the results of the measurement campaign. Spatial correlation, eigenvalue dispersion, capacity and DMT obtained from measured data are shown and analyzed. Sect. 5 gives the conclusion of the work.

2 Measurement

2.1 Equipment

An extensive measurement campaign was performed at center frequency of 4.9 GHz with 50 MHz effective bandwidth at Beijing University of Posts and Telecommunications (BUPT), Beijing, China. The Elektrobit PropSound Channel Sounder was employed, which is described in detail on http://www.propsim.com. The sounder works in a time-division multiplexing mode. Periodic pseudo random binary signals (PRBS) are transmitted between different Tx-Rx antenna pairs. The interval within which all sub-channels are sounded once is referred to as a measurement cycle. The uniform linear array (ULA) composed of eight antennas was utilized at both Tx and Rx firstly, which formed an 8×8 MIMO system. The antenna spacing is $\lambda/2$, where λ is the wavelength. To investigate the influence of antenna spacing on the MIMO system, the ULA composed of six 2λ-spaced antennas was then employed. The antenna pattern of utilized ULAs is obtained from Satimo SG128 antenna measurement system. Other important characteristics of measurement setup can be found in Table 1.

Table 1 Measurement parameters

Items	Settings
Carrier frequency/GHz	4.9
Effective bandwidth/MHz	50
Chip rate/MHz	100
Code length/chips	511
Tx power/dBm	26
Types of antennas	8×8 / 6×6 ULA
Antenna spacing	0.5λ / 2λ
Height of Tx antenna/m	2.5
Height of Rx antenna/m	1.8

2.2 Environment

The measurement was performed in the large hall on the first floor of a seven-floor building. Floors and the sidewalls of the corridor were covered with marbles. There were also several notice boards with glass sheets along both sides of the corridor. The layout of the hall is illustrated in Fig. 1. During the measurement, both the Tx and the Rx were mounted on the trolley. The star mark indicates the position where the Tx was fixed. Meanwhile, the Rx was moved to every spot denoted by red dot in the grid. At each spot, the broadside orientation of the Rx antenna was rotated to four different directions by 45°step in azimuth, i.e. 0°, ±45°and 90° relative to the initial broadside orientation, as shown in Fig. 1. For each Rx antenna position, 100 measurement cycles were transmitted and collected in each direction. In total, $40\times 100\times 4$=16 000 measurement cycles were obtained.

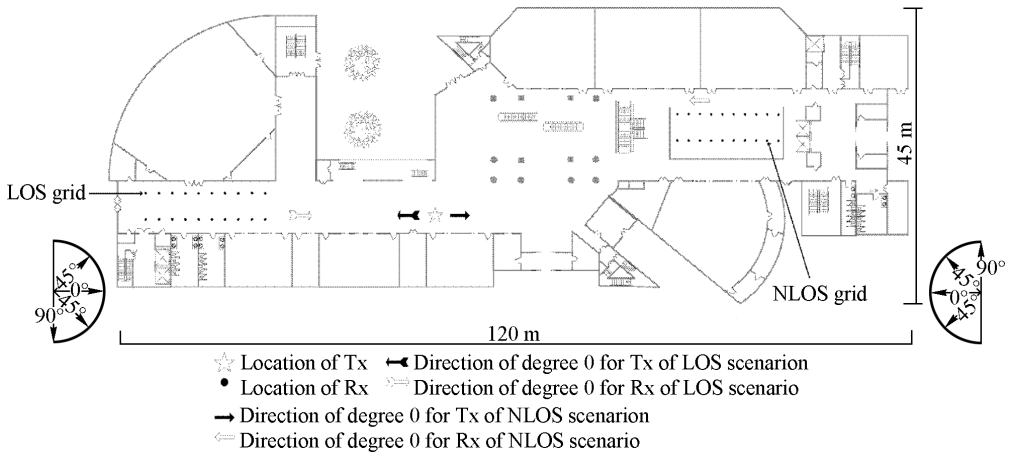

Note: Both the LOS and NLOS grids consist of 20 spots. The reference direction for rotating the broadside of the Rx antenna in LOS scenario is shown in the down-left corner, and the reference direction for NLOS scenario is shown in the down-right corner.

Fig. 1 Floor plan of indoor hotspot measurement scenarios

3 Data post-processing

Raw data collected by the Rx are the spread signals with the system impulse response of the sounding system. Raw data were cyclically correlated with the system impulse response, which was obtained from the calibration of the sounder, to remove the effect of the sounding system. Then, channel impulse responses (CIRs), i.e., $h(t,\tau)$ were calculated through the cyclic correlation with the known PRBS.

?1994-2014 China Academic Journal Electronic Publishing House. All rights reserved. http://www.cnki.net

Since the noise level P_n varies with time, the noise level estimation was done for each measurement cycle. To ensure that the signal is much stronger than the noise so that the additive noise does not affect the inherent characteristic of the channel, a threshold P_t was then determined by both the estimated noise level P_n and the peak power of CIRs, i.e., P_p

$$P_t = \max\{P_n + D_m, P_p - D_r\} \quad (1)$$

where D_m is the noise margin from noise floor P_n and D_r denotes the dynamic range from the peak power P_p. Paths with power $|h(t,\tau)|^2$ below the threshold level P_t were ignored. The dynamic range D_r was set to 25 dB and the margin D_m was set to 6 dB. By applying the Fourier transform to the remaining signal components, the corresponding frequency transfer functions $\boldsymbol{H}(t,f)$ can be obtained. As the spectrum of the transmitted signal reveals a sinc function, signal strength is weak at band edges. Therefore, only 50 MHz in the middle of the band was used for the computation. Assuming that the $\boldsymbol{H}(j,k)$ is the sample of $\boldsymbol{H}(t,f)$, one can obtain

$$\boldsymbol{H}(j,k) = \boldsymbol{H}(t,f)|_{t=j\Delta t, f=k\Delta f} = \boldsymbol{H}(j\Delta t, k\Delta f) \quad (2)$$

where Δt and Δf are the sampling intervals in time domain and frequency domain, respectively.

4 Measurement results and analysis

Based on the obtained CIRs, the most important characteristics of wideband MIMO channel, i.e., spatial correlation, the eigenvalue characteristics, capacity and DMT are investigated.

4.1 Spatial correlation

Correlation between the *m*th and *n*th receiver antennas can be calculated as

$$\rho_{m,n}^{\mathrm{Rx}} = \frac{\varepsilon\left[h_m h_n^*\right] - \varepsilon\left[h_m\right]\varepsilon\left[h_n^*\right]}{\sqrt{(\varepsilon[|h_m|^2] - |\varepsilon[h_m]|^2)(\varepsilon[|h_n|^2] - |\varepsilon[h_n]|^2)}} \quad (3)$$

where ε is the expectation over all transmitter antennas and * denotes the complex conjugate operation. Similarly, the correlation between *m*th and *n*th transmitter antennas can be calculated as

$$\rho_{m,n}^{\mathrm{Tx}} = \frac{\varepsilon\left[h_m h_n^*\right] - \varepsilon\left[h_m\right]\varepsilon\left[h_n^*\right]}{\sqrt{(\varepsilon[|h_m|^2] - |\varepsilon[h_m]|^2)(\varepsilon[|h_n|^2] - |\varepsilon[h_n]|^2)}} \quad (4)$$

where ε is the expectation over all receiver antennas. Using Eqs. (3) and (4), the correlation of both Rx and Tx side at integral multiples of antenna spacing can be obtained. Another method of calculating spatial correlation is using power azimuth spectrum (PAS). Given a distribution function $p(\phi)$ of PAS, the correlation can be calculated as

$$\rho(D) = \int_{\bar{\phi}-\sigma}^{\bar{\phi}+\sigma} \exp\{\mathrm{i}k_0 D\sin\phi\}\, p(\phi)\mathrm{d}\phi \quad (5)$$

where D is the antenna spacing, $k_0 = 2\pi/\lambda$ is the wavenumber in free space, $\bar{\phi}$ is the mean incidence angle, σ denotes the azimuth spread (AS) and i is the imaginary unit. Two of the most widely proposed distributions for PAS are the Laplacian and uniform function. 3GPP suggested a Laplacian distribution for the Tx PAS and either a Laplacian or a uniform distribution for the Rx PAS in its link-level calibration [8]. The Laplacian distribution is also adopted by Ref. [9] for modeling both the Tx and Rx PAS. Measured correlation coefficients are compared with correlation coefficients calculated from Laplacian and uniform PAS. 2000 cycles of measured data are used to estimate the correlation in LOS and NLOS scenario, respectively. From Figs. 2 and 3, it can be seen that in LOS scenario, the correlations of both the Tx and the Rx match with that obtained from the truncated Laplacian PAS with the AS σ equal approximately to 15°. In NLOS case, the correlation is significantly lower than that of LOS, which accounts for a larger AS. The correlation of Tx approximates to correlation calculated from truncated Laplacian PAS with σ equal to 80° and Rx manifests a similar correlation with the correlation produced by a uniform PAS. The probability distribution functions (PDFs) of PAS that produce similar spatial correlation with measured data and corresponding azimuth spreads are shown in Table 2. In the case of 6×6 ULA, since the antenna spacing is 2λ, the antennas exhibit rather low correlation. The results are not illustrated.

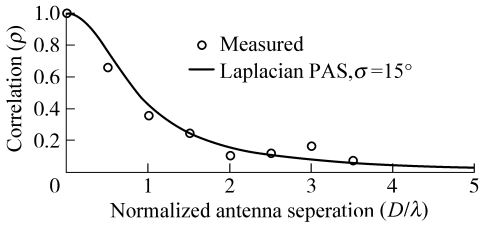

(a) Spatial correlation of Tx:LOS

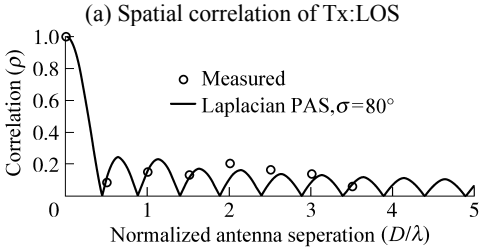

(b) Spatial correlation of Tx:NLOS

Fig. 2 Spatial correlations of Tx side obtained from the measured data and theoretical PAS as a function of antenna separation for both LOS and NLOS scenarios

?1994-2014 China Academic Journal Electronic Publishing House. All rights reserved. http://www.cnki.net

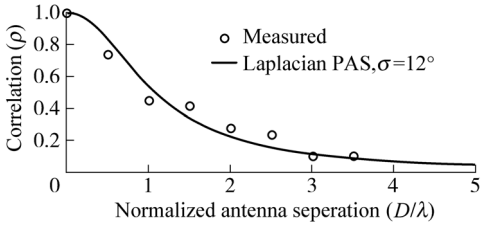

(a) Spatial correlation of Rx:LOS

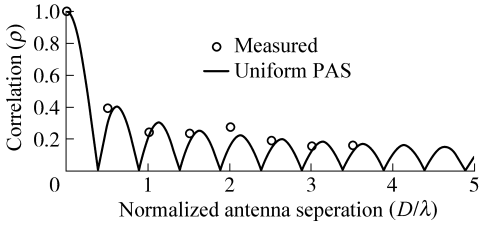

(b) Spatial correlation of Rx:NLOS

Fig. 3 Spatial correlations of Rx side obtained from the measured data and theoretical PAS as a function of antenna separation for both LOS and NLOS scenarios

Table 2 The PDF of PAS and corresponding AS

	LOS		NLOS	
	Tx	Rx	Tx	Rx
PDF of PAS	Laplacian	Laplacian	Laplacian	Uniform
AS (σ)	15°	12°	80°	104°

It can be observed from Table 2 that the power of MPCs occupies a large AS in NLOS scenario. This is because the barriers between Tx and Rx hamper paths heavily in NLOS scenario. Thereby, with high probability, MPCs transmit to the Rx via the reflection of side walls, ceiling and floor.

4.2 Eigenvalue dispersion

For any MIMO transfer matrix at the *k*th frequency bin of the *j*th time realization $\boldsymbol{H}(j,k)$, the singular value decomposition (SVD) can be obtained as

$$\boldsymbol{H}(j,k)=\boldsymbol{U}(j,k)\boldsymbol{\Sigma}(j,k)\boldsymbol{V}^{\mathrm{H}}(j,k)=\sum_{r=1}^{R}\lambda_r(j,k)\boldsymbol{u}_r(j,k)\boldsymbol{v}_r^{\mathrm{H}}(j,k) \tag{6}$$

where both the $N_{\mathrm{Rx}}\times N_{\mathrm{Rx}}$ matrix $\boldsymbol{U}$ and the $N_{\mathrm{Tx}}\times N_{\mathrm{Tx}}$ matrix $\boldsymbol{V}$ are unitary matrices, and $\boldsymbol{\Sigma}$ is a $N_{\mathrm{Rx}}\times N_{\mathrm{Tx}}$ diagonal matrix of singular values σ_i of $\boldsymbol{H}$. These singular values have the property that $\sigma_r=\sqrt{\lambda_l}$, where λ_l is the *l*th largest eigenvalue of $\boldsymbol{HH}^{\mathrm{H}}$. $\lambda_1(j,k)\geqslant\lambda_2(j,k)\geqslant...\geqslant\lambda_L(j,k))$, $1\leqslant L\leqslant\min(N_{\mathrm{Tx}},N_{\mathrm{Rx}})$, are the ordered eigenvalues of the *k*th frequency bin of *j*th time channel realization. *L* is the rank of channel. The eigenvalue dispersion (ED), which is an important metric of MIMO channel, is commonly used to characterize the relative differences between the powers of eigenvalues. In this article, S_{ED} is used as a measure of ED. The S_{ED} is defined as

$$S_{\mathrm{ED}}(j,k)=\frac{\left(\prod_{l=1}^{L}\lambda_l(j,k)\right)^{\frac{1}{L}}}{\frac{1}{L}\sum_{l=1}^{L}\lambda_l(j,k)} \tag{7}$$

which is the ratio of geometric and arithmetic means of the eigenvalues of $\boldsymbol{HH}^{\mathrm{H}}$. S_{ED} is a useful figure of merit to characterize ED by a single number [6]. It is noted that in the case of small ED, S_{ED} tends to unity ($S_{\mathrm{ED}}\to 1$), whereas, in the case of high ED, S_{ED} tends to zero ($S_{\mathrm{ED}}\to 0$).

The effect of antenna spacing on the ED is studied first. The 6×6 ULA produces smaller ED compared to 8×8 ULA for both LOS and NLOS case. It also can be found that the ED of NLOS scenario is significantly smaller than that of LOS scenario in the 8×8 ULA case, whereas, in the 6×6 ULA case, no significant difference is found between the LOS and NLOS scenario, as seen from Fig. 4. This is mainly because larger spacing between antennas results in relative more independent sub-channels for both LOS and NLOS scenario. For further investigation, the results of ED are studied as a function of antenna orientation in Fig. 5. For both

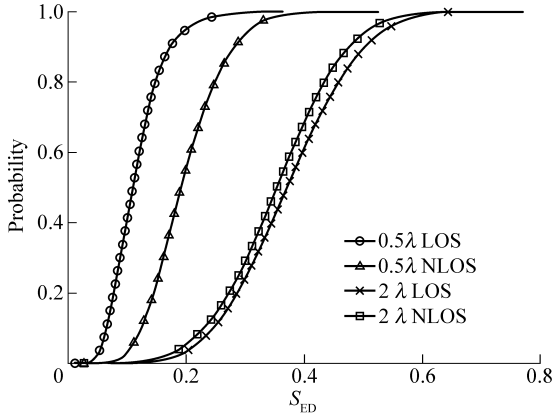

Fig. 4 Eigenvalue dispersion of ULA with respect to different antenna spacings. The antenna spacings are 0.5λ and 2λ, respectively

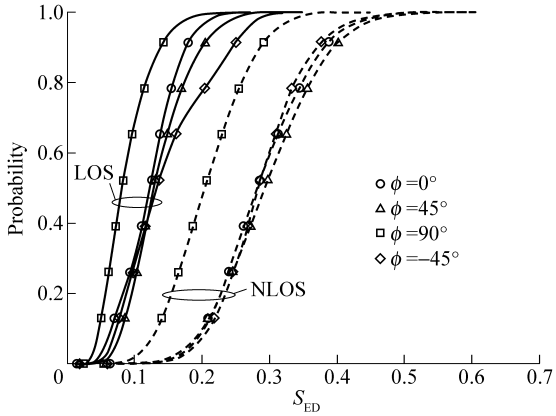

Fig. 5 Eigenvalue dispersion of 8×8 ULA with respect to different broadside orientations

?1994-2014 China Academic Journal Electronic Publishing House. All rights reserved. http://www.cnki.net

LOS and NLOS scenario, the maximum ED is produced when the broadside points to the direction of 90°. On the other hand, rotating the broadside to the directions of 0° and ±45° lead to similar EDs.

4.3 Capacity

Channel capacity is the main benefit resulted by applying MIMO for spatial multiplexing. The capacity of frequency-selective fading MIMO channel is given by Ref. [10].

$$C(t)=\frac{1}{B}\int_B \mathrm{lb}\,\det\left(\boldsymbol{I}_{N_{\mathrm{Rx}}}+\frac{\rho}{\beta N_{\mathrm{Tx}}}\boldsymbol{H}(t,f)\boldsymbol{H}^{\mathrm{H}}(t,f)\right)\mathrm{d}f \tag{8}$$

where ρ denotes the SNR and B is the bandwidth. For the discrete channel $\boldsymbol{H}(j,k)$, an approximation can be given by

$$C(j)\approx\frac{1}{K}\sum_{k=1}^{K}\mathrm{lb}\,\det\left(\boldsymbol{I}_{N_{\mathrm{Rx}}}+\frac{\rho}{\beta N_{\mathrm{Tx}}}\boldsymbol{H}(j,k)\boldsymbol{H}^{\mathrm{H}}(j,k)\right) \tag{9}$$

where K is the number of frequency bins of jth time realization and β is a common normalization factor for all channel realizations in such that the average channel power gain is unitary, i.e.,

$$\varepsilon\left\{\frac{1}{\beta}\|\boldsymbol{H}(j,k)\|_{\mathrm{F}}^2\right\}=N_{\mathrm{Rx}}N_{\mathrm{Tx}} \tag{10}$$

where ε is expectation operator over all channel realizations and $\|\cdot\|_{\mathrm{F}}$ denotes the Frobenius norm. The CIRs between different Tx-Rx antenna pairs are used to form the channel transfer matrix. After transforming the transfer matrix to the frequency domain, one can calculate the capacity using Eq. (9).

1) Capacity with respect to the broadside orientation

Cumulative distribution function (CDF) curves of capacity obtained from measurement with respect to array orientation are shown in Fig. 6. Consistent with the results of ED shown in Fig. 5, rotating the broadside to the direction of 90° shows the minimum capacity, meanwhile, similar capacity results are achieved with broadside pointing to 0° and ±45°.

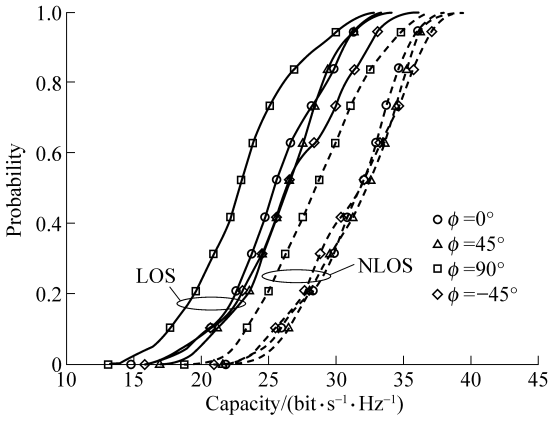

Fig. 6 Capacity of 8×8 ULA with broadside orientation pointing to the direction of 0°, ±45° and 90°. The SNR is 15 dB.

2) Capacity with respect to antenna spacing

Capacity CDF curves with different antenna spacings are compared in Fig. 7. The capacity of 8×8 ULA via channel selection is also illustrated. The channel selection is achieved by allocating equal power to the sub-channels with the largest six eigenvalues selected from all eight eigenvalues. Though showing larger ED, the 8×8 ULA with $\lambda/2$ spacing outperforms the 2λ spaced 6×6 ULA, which implies that increasing the number of antennas is more beneficial to the capacity improvement than increasing the antenna spacing in indoor hotspot environment. The capacity can be further improved through channel selection. It also shows evidence that there is no significant difference between the LOS and NLOS scenarios for the 2λ spaced antennas. However, this is not the case for $\lambda/2$ spaced antenna. The results indicate that larger antenna spacing is more robust against the variations of propagation conditions.

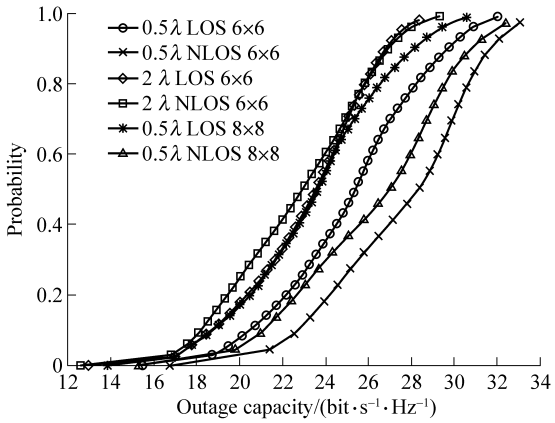

Fig. 7 Capacity of 6×6 ULA with 2λ antenna spacing, 8×8 ULA with $\lambda/2$, and capacity of 8×8 ULA after channel selection, where the SNR is 15 dB

4.4 Diversity-multiplexing tradeoff

The DMT characterizes the slow fading performance limit of the channel. The multiplexing gain r of MIMO channels is a measure of capability for supporting higher data rate than the single antenna channels, and the diversity gain d quantifies how sharply the outage probability decays as SNR grows. The theoretical derivation and analysis of DMT were reported in several literatures. In Ref. [11], the DMT of i.i.d. Rayleigh channel at high SNR was given by

$$d_\infty(r)=(N_{\mathrm{Rx}}-r)(N_{\mathrm{Tx}}-r);\quad 0\leqslant r\leqslant\min(N_{\mathrm{Rx}},N_{\mathrm{Tx}}) \tag{11}$$

Due to the imperfect factor in practical MIMO system, i.e., correlated fading and mutual coupling between antennas, the diversity gain will be reduced. The authors use the following scheme to investigate the DMT of the real propagation

?1994-2014 China Academic Journal Electronic Publishing House. All rights reserved. http://www.cnki.net

channel. At finite SNR, the multiplexing gain r is defined as the ratio of the data rate C to the capacity of an equivalent single antenna AWGN channel [12], i.e.,

$$r = \frac{C}{\mathrm{lb}(1+\rho)} \tag{12}$$

where ρ denotes the SNR. $p_{\mathrm{out}}(r,\rho)$, which is the outage probability as function of r and ρ, can be calculated from the measured channel as

$$p_{\mathrm{out}}(r,\rho) = \frac{1}{K}\sum_{k=1}^{K} I_{\mathrm{out}}(\rho,k) \tag{13}$$

where K is the total number of channel realizations, and $I_{\mathrm{out}}(\rho,k)$ is the indicator function defined by

$$I_{\mathrm{out}}(\rho,k)=\begin{cases}1; & \sum_{l=1}^{L}\mathrm{lb}(1+\rho\lambda_l(k)) < D_{\mathrm{r}} = \\ 0; & \text{otherwise}\end{cases}$$
$$\begin{cases}1; & \sum_{l=1}^{L}\mathrm{lb}(1+\rho\lambda_l(k)) < r\,\mathrm{lb}(1+\rho) \\ 0; & \text{otherwise}\end{cases} \tag{14}$$

where $\lambda_l(k)$ is the lth eigenvalue of kth channel realization. In practical operation, the diversity gain can be obtained for a range of D_{r} at different ρ as the negative gradients of the corresponding plots of $\mathrm{lb}\,p_{\mathrm{out}}$ against $\mathrm{lb}\,\rho$. The DMT of measured channels, along with $d_\infty(r)$ are given in Figs. 8 and 9. Note that the diversity gain of measured channel at $r=0$ cannot be calculated since the capacity of measured channel is always greater than zero.

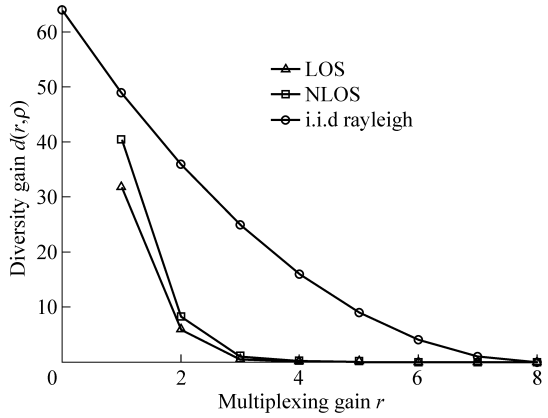

Fig. 8 DMT for 8×8 ULA with $\lambda/2$ spacing, where the SNR is 15 dB

As shown in Figs. 8 and 9, the measured channels at operational SNR of 15 dB have a much lower tradeoff than the theoretical results $d_\infty(r)$ of i.i.d. Rayleigh channel, which accounts for the correlation between antennas. Furthermore, channels in NLOS propagation environment provide higher tradeoff in contrast to LOS channels. Comparing the results in Figs. 8 and 9, it can also be found that the difference between measured tradeoff and $d_\infty(r)$ decreases as the antenna spacing increases. This is mainly caused by the increment of antenna spacing, which reduces the impact of spatial correlation.

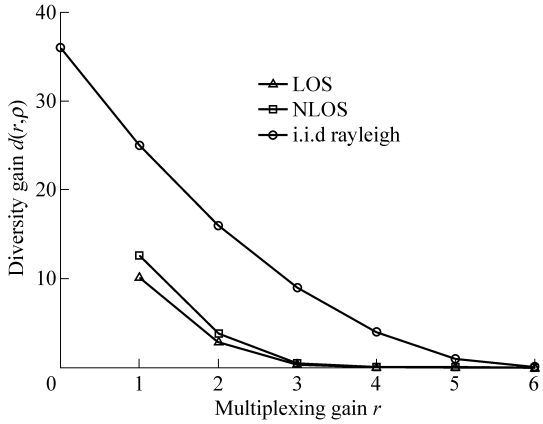

Fig. 9 DMT for 6×6 ULA with 2λ spacing, where the SNR is 15 dB

5 Conclusions

This article presents the results from wideband channel measurements at 4.9 GHz of an indoor hotspot scenario. For LOS scenario, the spatial correlations of both Tx and Rx match the correlation values obtained from the Laplacian PASs, and the correlation values of Tx and Rx in NLOS scenario well agree with the correlation produced by the Laplacian and uniform PAS, respectively. Then, the eigenvalue dispersion and capacity with respect to the antenna spacing and orientation are presented. It is found that there is no significant difference in eigenvalue dispersion and capacity with the broadside pointing to the direction of $0°$ and $\pm 45°$. However, when the broadside points to the direction of $90°$, the ED becomes larger and results in a relatively low capacity. The DMT at operational SNR are then studied. Due to the spatial correlation, the measured channels at SNR of 15 dB manifest a much lower DMT than the DMT of i.i.d. Rayleigh. Increasing the antenna spacing can alleviate the impact of spatial correlation on degradation of optimal tradeoff. These results obtained from measurement provide important basis for future studies of indoor hotspot propagation characteristics and MIMO system designs.

Acknowledgements

This work was supported by the China Important National Science and Technology Specific Projects (2009ZX03007-003-01), the

?1994-2014 China Academic Journal Electronic Publishing House. All rights reserved. http://www.cnki.net

Hi-Tech Research and Development Program of China (2009AA011502).

References

1. Foschini G J, Gans M J. On limits of wireless communications in a fading environment when using multiple antennas. Wireless Personal Communications, 1998, 6(3): 311–335
2. Telatar I E. Capacity of multi-antenna Gaussian channels. European Transactions on Telecommunications, 1999, 10(6): 585–595
3. Ali A R, Ali A A, Omar A S. High resolution WLAN indoor channel parameter estimation and measurements for communication and positioning applications at 2.4, 5.2 and 5.8 GHz. Proceedings of Radio and Wireless Symposium (RWS'06), Jan. 17–19, 2006, San Diego, CA, USA. Psicataway, NJ, USA: IEEE, 2006: 79–282
4. Hamalainen J, Wichman R, Nuutinen J P, et al. Analysis and measurements for indoor polarization MIMO in 5.25 GHz band. Proceedings of the 61st Vehicular Technology Conference (VTC-Spring'05): Vol 1, May 30–Jun 1, 2005, Stockholm, Sweden. Piscataway, NJ, USA: IEEE, 2005: 252–256
5. Jalden N, Zetterberg P, Ottersten B, et al. Correlation properties of large scale fading based on indoor measurements. Proceedings of Wireless Communications and Networking Conference (WCNC'07), Mar 11–15, 2007, Hong Kong, China. New York, NY, USA: EEE, 2007: 1894–1899
6. Suvikunnas P, Salo J, Vuokko L, et al. Comparison of MIMO antenna configurations: methods and experimental results. IEEE Transactions on Vehicular Technology, 2008, 57(2): 1021–1031
7. Kafle P L, Intarapanich A, Sesay A B, et al. Spatial correlation and capacity measurements for wideband MIMO channels in indoor office environment. IEEE Transactions on Wireless Communications, 2008, 7(5): 1560–1571
8. Spatial channel model for MIMO simulations. 3GPP TR 25.996 V7.0.0. 2007
9. IEEE 802 11-03/161r2. TGn indoor MIMO WLAN channel models. 2003
10. Paulraj A, Nabar R, Gore D. Introduction to space-time wireless communications. Cambridge, UK: Cambridge University Press, 2003
11. Zheng L Z, Tse D N C. Diversity and multiplexing: a fundamental tradeoff in multiple-antenna channels. IEEE Transactions on Information Theory, 2003, 49(5): 1073–1096
12. Narasimhan R. Finite-SNR diversity-multiplexing tradeoff for correlated Rayleigh and Rician MIMO channels. IEEE Transactions on Information Theory, 2006, 52(9): 3965–3979

(Editor: WANG Xu-ying)

?1994-2014 China Academic Journal Electronic Publishing House. All rights reserved. http://www.cnki.net